PROCEEDINGS OF SPIE

SPIEDigitalLibrary.org/conference-proceedings-of-spie

Optimized piezoelectric energy harvesters for performance robust operation in periodic vibration environments

Wen Cai, Ryan L. Harne

Wen Cai, Ryan L. Harne, "Optimized piezoelectric energy harvesters for performance robust operation in periodic vibration environments," Proc. SPIE 10967, Active and Passive Smart Structures and Integrated Systems XII, 109670M (21 March 2019); doi: 10.1117/12.2514041



Event: SPIE Smart Structures + Nondestructive Evaluation, 2019, Denver, Colorado, United States

Optimized Piezoelectric Energy Harvesters for Performance Robust Operation in Periodic Vibration Environments

Wen Cai and Ryan L. Harne*
Department of Mechanical and Aerospace Engineering, The Ohio State University, Columbus, OH 43210, USA

ABSTRACT

Energy harvesters with wide frequency range, long lifetime, and high output power are preferred to serve as power supplies for wireless devices. Motivated to guide the design of a robust energy harvesting platform, an analytical model based on the Euler-Bernoulli beam theory for a laminated beam is first presented to predict the nonlinear response of the system when subjected to harmonic base acceleration and tunable magnetic forces. Following experimental validation, a multi-objective optimization based on a genetic algorithm considers how to improve the frequency range of high performance, decrease peak strain level, and maximize output power by manipulating the design of the nonlinear energy harvester. The optimization results indicate that a slightly monostable configuration is superior when taking all three aspects into consideration.

1. INTRODUCTION

It is of great importance to optimize piezoelectric harvester platforms to deliver performance-robust operation over a long time horizon [1]. The optimization of piezoelectric energy harvesters has been addressed through a variety of strategies to date. Following efforts that studied concepts of beam tapering to prescribe beam strain distributions [2], later efforts considered the beam shape, especially tapering along the length, to tailor for linear dynamic response of piezoelectric energy harvesters [3]. It has been shown that piezoelectric cantilevers that have reduced width tapers from clamped end to free tip deliver greater specific electrical power than rectangular cantilevers [4]. Additional characteristics such as partial electrode or partial piezoelectric material placement along the length of a beam [5] [6] [7] have recommended avoidance of strain nodes for effective energy harvesting in linear dynamic regimes when considering multimodal vibration response.

More recent attention has been given to optimizing piezoelectric energy harvesters in light of factors essential to practical operations but posing genuine fundamental scientific questions. For instance, a study on optimizing harvesters for human kinetic energy harvesting by tailoring the beam orientation shed light on how the complex, multi-directional excitation profile on the piezoelectric cantilever contributes to the resulting output power [8]. In addition, an accounting of large nonlinear deformations exhibited by piezoelectric cantilevers indicates that material strength limitations may conflict with optimization based purely on output power generation [9]. Such more transparent modeling also reveals that linear models may be wholly unable to capture the realities of kinetic energy conversion associated with nonlinear deformation [10].

Despite these advancements, significant optimization efforts remain to deliver high-performing, robust-operation, and long-life service that would provide the self-sustaining power supplies needed for IoT applications. In particular, piezoelectric beams may be made more mechanically robust through lamination to provide effective electrical voltage [11]. Lamination introduces complex relations between cantilever bending and strain fields. Yet, such laminated harvester designs have not been optimized in the literature. The performance-enhancing nonlinearities [9] have not yet considered bistable and essential nonlinearities of single piezoelectric cantilevers that are known to enhance robustness [12] [13].

Consequently, this research devises an optimization tool for nonlinear piezoelectric energy harvesters created from laminated beam designs and interfaced with a resistive electrical load. The following sections first introduce the

_

^{*} Correspondence to: harne.3@osu.edu

analytical method to model the laminated piezoelectric and beam with magnetic nonlinearities. Then after identifying the system parameters experimentally, an optimization method based on genetic algorithm is proposed to discover optimal combination of beam length and distance between magnets.

2. MODEL FORMULATION AND SOLUTION

A typical nonlinear energy harvesting system connected to a load resistance R is shown in Figure 1(a). The piezoelectric beam, whose length and width are L and b respectively, is clamped at one end. A mass M_0 consisting of the mass of the magnet and the holder is added to the beam free end. In the following derivation, the magnet holder is taken as a rigid extension to the piezoelectric beam free end. The length of the holder extension is d_1 . A repulsive magnet is mounted next to the beam free end to introduce nonlinearity. The distance between two magnets is d_2 . In addition, as shown in Fig. 1(b), the piezoelectric beam here is composed of nine layers. The materials for the layers are FR4, copper, PZT-5H, copper, PZT-5H, copper, and FR4. FR4 is a glass fiber-reinforced epoxy laminate used to enhance durability by the layering around the more brittle PZT-5H. The thicknesses of FR4 layer, copper layer, and PZT layer are $2h_s$, h_c , h_p respectively. The two piezoelectric layers are connected in parallel.

Since only the fundamental frequency vibration is considered, which is dominated by the transverse vibration, Euler-Bernoulli beam theory is adopted to approximate the strain distribution. When the transverse displacement at the free end of the beam is w(x,t), the strain distribution including the geometry nonlinearity [14] is written as

$$S_{1} = -z \left[w_{xx} \left(1 - w_{x}^{2} \right)^{-1/2} \right] \Box - z w_{xx} \left(1 + \frac{1}{2} w_{x}^{2} \right) \tag{1}$$

The w_x represents for $\frac{\partial w}{\partial x}$, w_{xx} is the corresponding second derivative. z is the distance away from the neutral axis, the subscript 1 means the strain in the x direction.

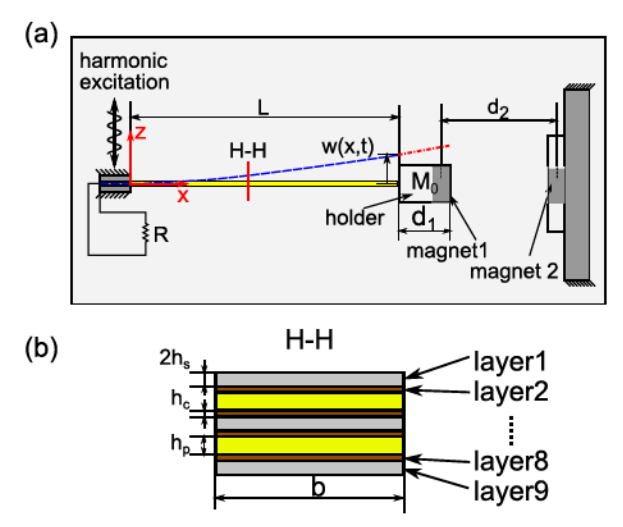


Figure 1. (a) Schematic of nonlinear energy harvester with repulsive magnets (b) layers of the piezoelectric beam For the two piezoelectric layers, the electrical potential $\varphi(z,t)$ is assumed to be a linear function only varying with z location [15] [16]. E_3 is the corresponding electrical field in the z direction, which is a constant inside the piezoelectric layers and can be calculated from $\varphi(z,t)$.

$$E_3 = -\frac{\partial \varphi}{\partial z} = -\varphi_z \tag{2}$$

Since Euler-Bernoulli beam theory is adopted here, the mechanical and electrical coupling for the piezoelectric layers can be simplified to be

$$\begin{bmatrix} D_3 \\ T_1 \end{bmatrix} = \begin{bmatrix} \mathcal{E}_{33}^s & \mathcal{E}_{31} \\ -\mathcal{E}_{31} & \mathcal{E}_p \end{bmatrix} \begin{bmatrix} \mathcal{E}_3 \\ \mathcal{S}_1 \end{bmatrix}$$
 (3)

Where D_3 is the electric displacement in z direction, T_1 and S_1 are the stress and strain in x direction. e_{31} refers to the coupling effect caused by the electrical field in z direction on the stress in x direction, ε_{33}^s defines the absolute dielectric matrix at constant strain, E_p is the Young's modulus of the material.

An energy-based method of deriving the equations of motion for the system is employed using Euler-Lagrange equations with the Ritz method. For sake of brevity, the details of the derivation are not included here. Assuming that the vibration responses for the generalized mechanical and electrical coordinates are independent in space and time, then the mechanical response is approximated by (4) and the electrical response is approximated by (5a).

$$w(x,t) = \mathbf{\psi}(x)\mathbf{r}(t) = \left[\psi_1(x) \quad \cdots \quad \psi_M(x)\right] \begin{bmatrix} r_1(t) \\ \vdots \\ r_M(t) \end{bmatrix} = \sum_{i=1}^N \psi_i r_i$$
(4)

$$\varphi(z,t) = \mathbf{\Phi}(\mathbf{z})\mathbf{v}(\mathbf{t}) = \left[\Phi_1(z) \quad \Phi_2(z)\right] \begin{bmatrix} v_1(t) \\ v_2(t) \end{bmatrix} = \sum_{q=1}^2 \Phi_q v_q$$
(5a)

$$\Phi_{1}(z) = \begin{cases}
\frac{z - h_{s} - h_{c}}{h_{p}}; & h_{s} + h_{c} \leq z \leq h_{s} + h_{p} + h_{c} \\
0 & elsewhere
\end{cases}$$
(5b)

$$\Phi_{2}(z) = \begin{cases}
-\frac{z + h_{s} + h_{c}}{h_{p}}; & -(h_{s} + h_{p} + h_{c}) \leq z \leq -h_{s} - h_{c} \\
0 & elsewhere
\end{cases}$$
(5c)

The M is the total number of functions for the mechanical generalized coordinates. The $r_i(t)$ is the corresponding generalized displacement. The mode shapes of the cantilever [17] are taken as trial functions $\psi_i(x)$. The v_q represents the physical voltage at the piezoelectric electrodes. The potentials at $z = h_s + h_c$ and $z = -(h_s + h_c)$ are set to be zero as grounded. Once the (4) and (5) are substituted into the components of the Lagrangian for the system, the corresponding Euler-Lagrange equations lead to (6a) and (6b)

$$[M]\ddot{\mathbf{r}} + [D]\dot{\mathbf{r}} + [K]\mathbf{r} + [K_1]\mathbf{r} + \mathbf{F}_{NL1} + [\Theta_1]\mathbf{v} + \mathbf{F}_{NL2} = \mathbf{f}_{m}$$
(6a)

$$-\left[\Theta_{I}\right]\dot{\mathbf{r}} + \dot{\mathbf{F}}_{NL3} + \left[C_{p}\right]\dot{\mathbf{v}} - \left[f_{e}\right]\mathbf{v} = 0 \tag{6b}$$

The terms in (6a,b) are omitted here for sake of brevity.

Principles of harmonic and stochastic linearization are utilized to linearize the original governing equations [18][19]. The linearized governing equations are consolidated to be

$$\left[\tilde{M}\right]\ddot{\mathbf{x}} + \left\{\left[\tilde{D}\right] + \left[\tilde{K}_{e}\right]^{(\theta_{3})}\right\}\dot{\mathbf{x}} + \left[\tilde{K}\right]\mathbf{x} + \left\{\left[\tilde{K}_{e}\right]^{(k_{3})} + \left[\tilde{K}_{e}\right]^{(\theta_{2})}\right\}\mathbf{x} = \tilde{\mathbf{f}}$$

$$(7)$$

Assuming a harmonic excitation is applied to the system, the force vector in the governing equation (7) can be written as

$$\tilde{\mathbf{f}} = \mathbf{F}e^{j\omega t} \tag{8}$$

By virtue of the periodic excitation, periodic response is assumed. Due to the linearization, the generalized coordinates are all together assumed to be composed of complex exponentials and constant, bias terms. By substitution of the assumed solutions into (7) and collecting together harmonic and constant terms, a sequence of algebraic equations is obtained that is solved to determine the dynamic response of generalized displacements and generalized voltages.

3. EXPERIMENTAL VALIDATION

Figure 2 shows a photograph of the experimental platform. A piezoelectric beam (PPA-2014, Mide Technology) is clamped on an electrodynamic shaker (APS Dynamics 400) with a plastic holder and a neodymium magnet at the free end. The driven force applied to harmonically accelerate the table is provided by a controller (Vibration Research Controller VR9500) and amplifier (Crown XLS 2500). An accelerometer (PCB Piezotronics 333B40) is used to provide feedback for the controller to ensure a constant base acceleration amplitude. Laser displacement sensors (Micro-Epsilon ILD-1420) are installed to measure the absolute displacements of the beam tip and shaker table as shown in Fig. 2. In experiment, by adjusting the position of the magnet 2 the nonlinear effect included in the system is changed from monostable to bistable.

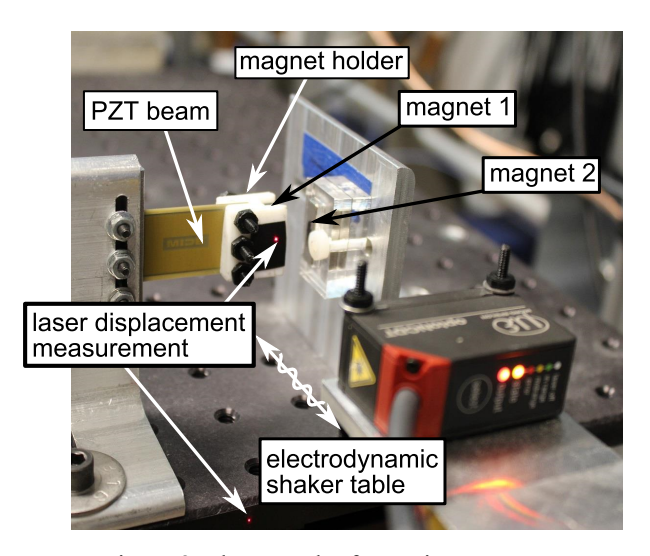


Figure 2. Photograph of experiment setup

Table 1. Experimentally identified system parameters.

L (mm)	b (mm)	h_s (mm)	h_p (mm)	h_c (mm)	d_1 (mm)	а	b
32	20.8	0.04	0.19	0.01	10	0.25	0.68
M_0 (g)	$R(k\Omega)$	M_a (MA/m)	V(cm ³)	$\alpha (\times 10^{-5})$	$\beta (\times 10^{-5})$	$a_z \text{ (m/s}^2\text{)}$	
10.32	100	1.61	0.768	8	8	7.5	

Table 2. Material properties for different layers

E_s (GPa)	E_p (GPa)	E_c (GPa)	ρ_s (kg/m ³)	$\rho_p (\text{kg/m}^3)$	$\rho_c (\text{kg/m}^3)$	ε_{33} (nF/m)	$e_{31} (C/m^2)$
26	60.6	128	1900	7800	940	3.16	-16.6

In order to validate the analytical model presented in Sec. 2, four positions of magnet 2 are considered. The parameters used in the analysis are identified from experiments and listed in Tables 1 and 2. Figure 3 presents the beam tip displacement amplitude and output voltage at different excitation frequency under the same excitation acceleration amplitude 7.5 m/s² for both the monostable and bistable configurations. At the frequency far away from the resonance, the experiment data indicates a lower amplitude comparing with the analysis. One explanation for this effect is that the piezo beam used in the experiment practically exhibits viscoelastic damping. At higher frequencies such as around 36 Hz, experiment and analysis also show minor disagreement, which may be associated with dynamics of the shaker table resonance. Despite the differences stated above, both experiments and analysis show the same trend while adjusting the magnet 2 position. When the distance between two magnets is larger than 16mm, the interaction of two magnets leads to a monostable configuration. With the decrease of d_2 , the resonance frequency will be decreased. Further decreasing the distance d_2 to be less than 14.8mm, the harvesting system becomes a bistable one. Then the decrease in the distance d_2 will increase the resonance frequency instead. In addition, both mechanical and electrical responses around the resonance are identical experimentally and analytically. Ignoring two cases resonating around 36 Hz, as shown in Table. 3, the other two cases show great agreement in bandwidth and RMS value of the voltage inside the bandwidth, which further help validate the model formulation and solution efforts and build the confidence to utilize the model in optimization.

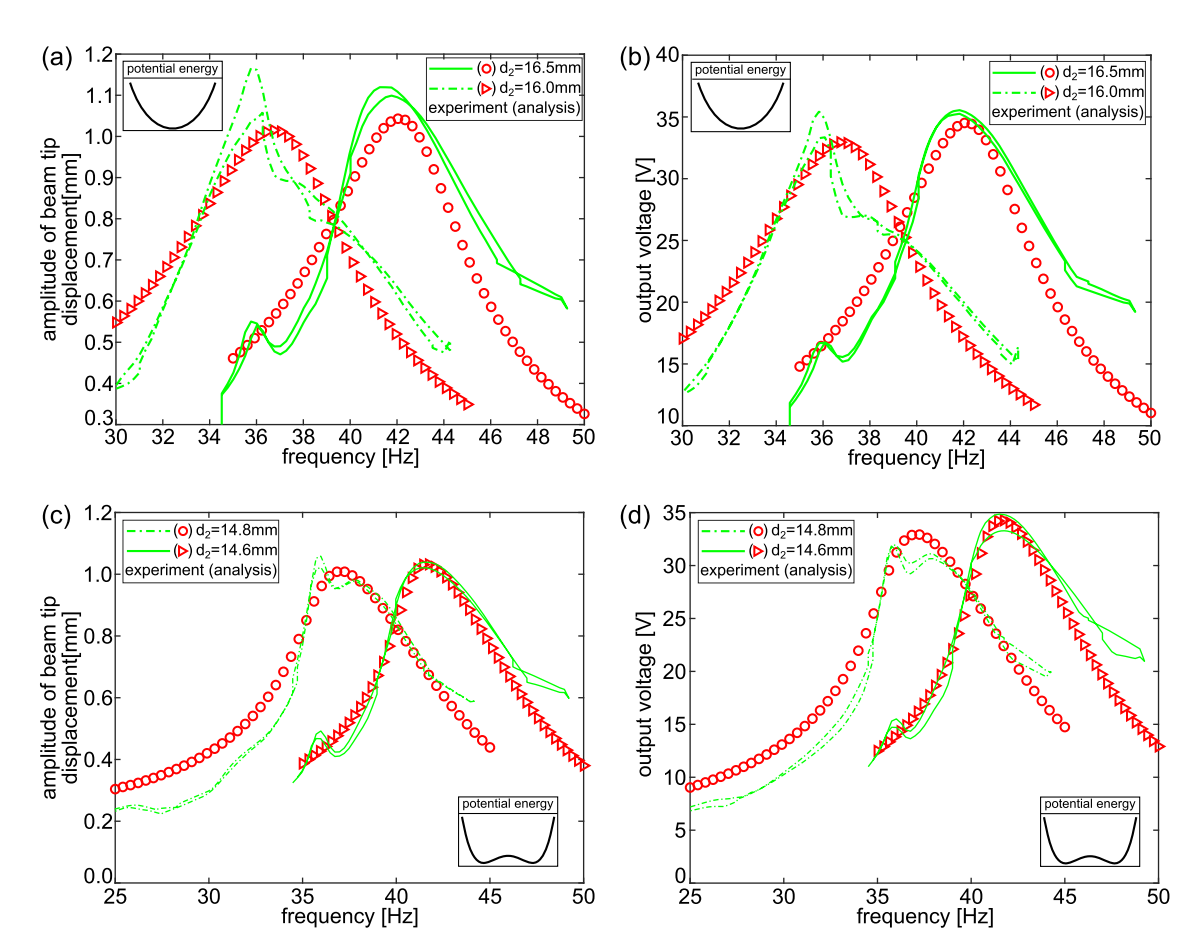


Figure 3. Mechanical and electrical response of (a) beam-tip displacement amplitude and (b) output voltage for a monostable system at different excitation frequency; (c) and (d) corresponding results for a bistable system.

Table 3. Analytical and experimental results comparison

	$d_2 = 16.5 \text{ mm}$		$d_2 = 14.6 \mathrm{mm}$		
	Analysis	Experiment	Analysis	Experiment	
Bandwidth (Hz)	6.13	6.00	6.06	6.75	
RMS value of voltage (V)	30.18	31.67	30.13	30.54	

4. OPTIMIZATION FOR ROBUST ENERGY HARVESTER SYSTEM

An energy harvester is desired to provide self-sufficient electrical energy on a near-continuous basis. Therefore, in this research a multi-objective optimization tool based on the genetic algorithm (GA) is devised to guide attention to robust energy harvesters.

The energy harvester is usually installed in a confined, packaged space to provide sustainable power supply. Then, the constraint on the beam length L_{max} is set as 80 mm. Therefore beam length L and magnet distance d_2 are chosen as design variables. The constraints are

- 1. $L + d_2 < L_{\text{max}} + d_1$
- 2. $45mm \le L \le 52mm$
- 3. $18mm < d_2 < 23mm$

The first constraint is from the limitation in the beam length. The minimum beam length should ensure that snap-through response can happen under the fixed acceleration amplitude, which also determine the minimum value for the magnets distance d_2 to avoid exceedingly high nonlinearity in system. The corresponding maximum beam length is equal to $L_{\max} - \min(d_2)$. The maximum value for d_2 is defined to introduce enough monostable effect to the system. With these parameter limitations, a continuous GA [25] is devised on the basis of multi-objective optimization for the following performance metrics.

- 1. Frequency range f_{range} , which is calculated based on the definition of bandwidth from the beam tip displacement response.
- 2. The RMS value of output voltage V_{rms} . Only the values on the high branch inside the frequency range will be added together to form the cost function for the voltage aspect.
- 3. The RMS value of strain at the fixed end S_{rms} . For a bistable system, static bias will greatly influence the fatigue life of the beam. Since when considering multiple degree of freedom in the governing equation, it is challenging to realize the stability check. Here instead of only adding the strain on the high branch (snapthrough) inside the frequency range, all the values for the intrawell response will also be added to build the strain cost function.

It is necessary to non-dimensionalize each objective function. The specific values for such normalization are

$$f_0 = 25 \text{ Hz}, \ V_0 = 65 \text{ V}, \ S_0 = 1365 \,\mu\text{s}$$
 (9)

Therefore, the multi-objective cost function is

$$\cos t = -\left(w_f \cdot \frac{f_{range}}{f_0} + w_v \cdot \frac{V_{rms}}{V_0}\right) + w_s \cdot \frac{S_{rms}}{S_0}$$
(10)

Where

$$w_f + w_v + w_s = 1 \tag{11}$$

In this work, a total of 60 generations are used in the optimization where each population size is 50. From one generation to the next, the selection rate is set to be 50% and the mutation rate is 20%.

First the weights for different cost functions are set to be equal, which is 0.333. With the setting described in Sec. 4, a monostable configuration with L = 45.88 mm and $d_2 = 18.43$ mm is outstanding after a massive calculation. In order to validate the optimization design and learn the role that nonlinearity play in a harvester system, the other three cases with same beam length and different magnet distance are studied. One more case with longer beam length is also presented as a comparison in beam length.

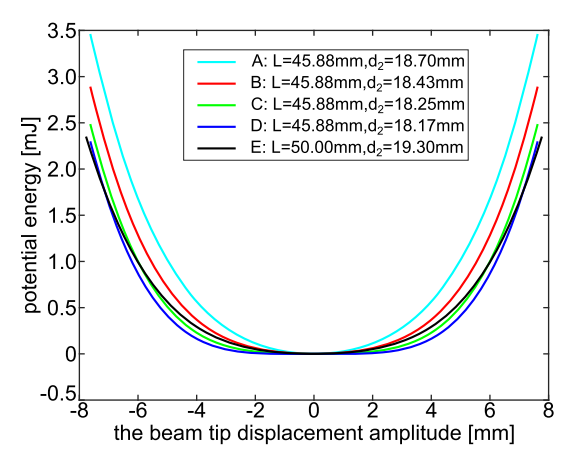


Figure 4. Potential energy for different configurations

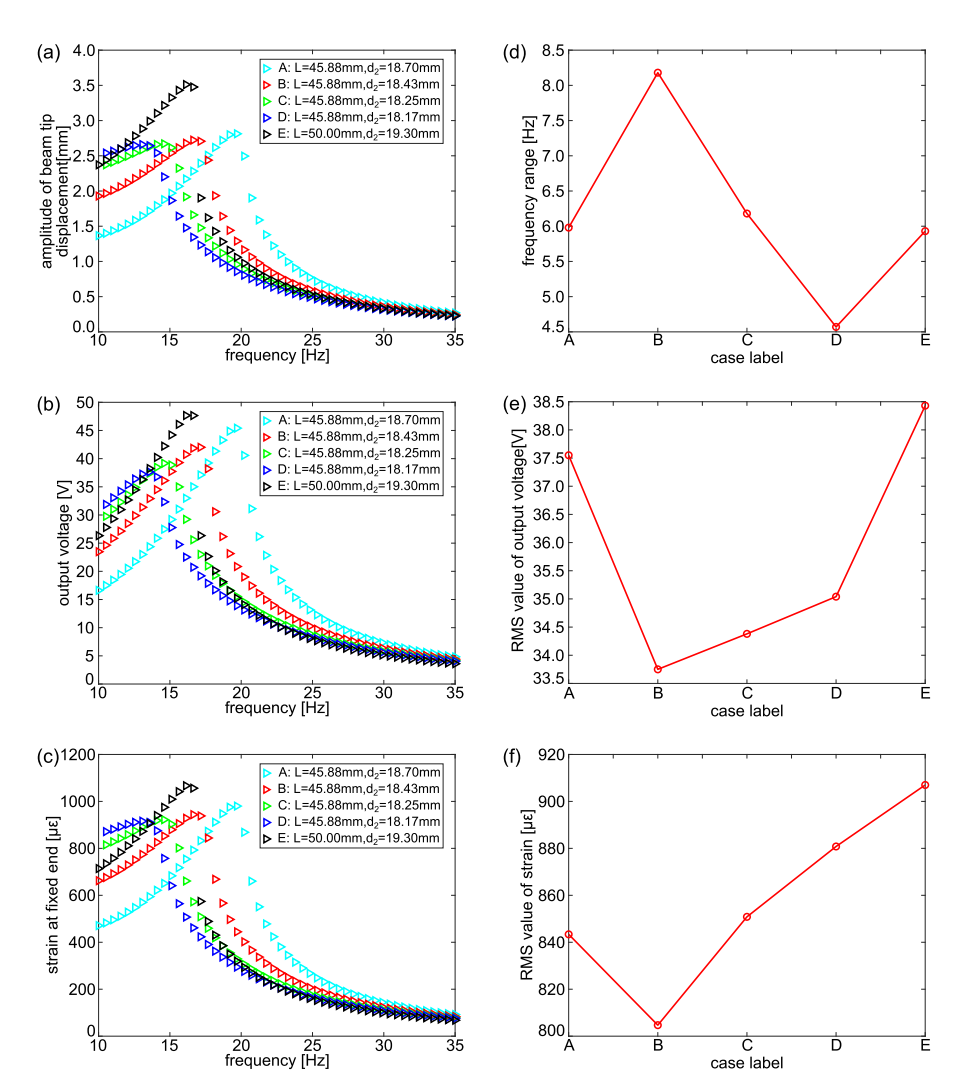


Figure 5. (a) Amplitude of beam tip displacement (b) output voltage (c) strain at the fixed end at different excitation frequency under the acceleration amplitude 7.5 m/s², (e) frequency range calculated from the mechanical response based on the concept of bandwidth, (e) the RMS value of voltage inside the frequency range, (f) the RMS value of strain at the fixed end inside the frequency range

As shown in Figure 4, case B is the optimal design from the GA codes, which is a monostable system. Then decreasing the magnet distance, case C will be around the neutral nonlinear condition. Further decreasing the magnets distance, from the plot of the potential energy, case D becomes a slightly bistable configuration. Case A is to increase the magnet distance on the basis of case B, which is also a monostable case. Besides, case E, a longer beam with a minor magnet distance, is also proposed. Figure 5(a,b,c) display the corresponding displacement response, output voltage, and the strain response at the fixed end, the corresponding value of three objectives for the five cases are shown in Fig. 5(d,e,f). From Fig.5 (d), with the decrease of magnet distance, the frequency range will first increase then decrease, the maximum frequency range exists in case B. Based on the mechanical response in Fig.5(a), a wider frequency range is corresponding to a lower displacement amplitude, which will result in a lower strain level and lower output voltage as shown in Fig 5(e) and (f). Comparing the first four cases, case B predicts a wider frequency range and lower strain level. Although the RMS value for output voltage is not as high as the value in the other cases, the difference is pretty small, which makes case B the optimal design and also indicates that a least monostable configuration is preferred in a robust nonlinear harvester design. In addition, from Fig. 5(e) a large magnet distance and long beam length will highly increase the RMS value of the voltage. The comparison between different cases validates the optimal design and shows the reasonability of the optimization tool proposed before.

5. CONCLUSION

This research studies the optimization of a nonlinear piezoelectric energy harvester with magnetic nonlinearity. An analytical model is first derived to predict the nonlinear dynamic behavior of the laminated piezoelectric beam. Experiments show good agreement with the analysis in both bandwidth and output power, which helps validate the analytical model. Then using genetic algorithm optimization, a multi-objective optimization problem is formulated to consider the frequency range, output power, and strain level of energy harvester system geometries. The optimization result indicates that to balance the three influences in the optimization, a slightly monostable configuration is preferred.

ACKNOWLEDGEMENTS

This research is supported by the National Science Foundation under Award No. 1661572. The authors are grateful to additional hardware support from Midé Technology.

REFERENCES

- [1] Gorlatova M., Sarik J., Grebla G., Cong M., Kymissis I., and Zussman G., "Movers and shakers: kinetic energy harvesting for the internet of things," IEEE Journal on Selected Areas in Communications, 33, 1624-1639 (2015).
- [2] Baker J., Roundy S., and Wright P. 2005 Alternative geometries for increasing power density in vibration energy scavenging for wireless sensor networks. In *Proceedings of 3rd International Energy Conversion Engineering Conference*; San Francisco. AIAA 2005-5617.
- [3] Dietl J.M., Garcia E., "Beam shape optimization for power harvesting," Journal of Intelligent Material Systems and Structures, **21**, 633-646 (2010).
- [4] Benasciutti D., Moro L., Zelenika S., and Brusa E., "Vibration energy scavenging via piezoelectric bimorphs of optimized shapes," Microsystems Technologies, **16**, 657-668 (2010).
- [5] Pillai M.A., Ebenezer D.D., and Deenadayalan E., "Design and optimization of piezoelectric unimorph beams with distributed excitation," The Journal of the Acoustical Society of America, **143**, 2685-2696 (2018).
- [6] Wang Q., Wu N., "Optimal design of a piezoelectric coupled beam for power harvesting," Smart Materials and Structures, **21**, 085013 (2012).
- [7] Acciani G., Dimucci A., and Lorusso L., "Multimodal piezoelectric devices optimization for energy harvesting," International Journal of Multiphysics, 7, 227-243 (2013).
- [8] Izadgoshasb I., Lim Y.Y., Lake N., Tang L., Padilla R.V., and Kashiwao T., "Optimizing orientation of piezoelectric cantilever beam for harvesting energy from human walking," Energy Conversion and Management, 161, 66-73 (2018).
- [9] Upadrashta D., Yang Y., and Tang L., "Material strength consideration in the design optimization of nonlinear energy harvester," Journal of Intelligent Material Systems and Structures, **26**, 1980-1994 (2015).
- [10] Patel R., McWilliam S., and Popov A.A., "Optimization of piezoelectric cantilever energy harvesters including non-linear effects," Smart Materials and Structures, 23, 085002 (2014).
- [11] Sodano H.A., Inman D.J., and Park G., "Comparison of piezoelectric energy harvesting devices for recharging batteries," Journal of Intelligent Material Systems and Structures, **16**, 799-807 (2005).
- [12] Harne R.L., Wang K.W., "Prospects for nonlinear energy harvesting systems designed near the elastic stability limit when driven by colored noise," ASME Journal of Vibration and Acoustics, **136**, 021009 (2014).

- [13] He Q., Daqaq M.F., "New insights into utilizing bistability for energy harvesting under white noise," Journal of Vibration and Acoustics, 137, 021009 (2015).
- [14] Harne R.L., Wang K.W., "Axial suspension compliance and compression for enhancing performance of a nonlinear vibration energy harvesting beam system," Journal of Vibration and Acoustics, **138**, 011004 (2016).
- [15] Hagood N.W., Chung W.H., and Von Foltow A., "Modelling of piezoelectric actuator dynamics for active structural control," Journal of Intelligent Material Systems and Structures, 1, 327-354 (1990).
- [16] Goldschmidtboeing F., Woias P., "Characterization of different beam shapes for piezoelectric energy harvesting," Journal of micromechanics and microengineering, **18**, 104013 (2008).
- [17] Erturk A., Inman D.J., "An experimentally validated bimorph cantilever model for piezoelectric energy harvesting from base excitations," Smart materials and structures, **18**, 025009 (2009).
- [18] Spanos P.D, "Stochastic linearization in structural dynamics," Applied Mechanics Reviews, 34, 1-8 (1981).
- [19] Harne R.L., Goodpaster B.A., "Impedance measures in analysis and characterization of multistable structures subjected to harmonic excitation," Mechanical Systems and Signal Processing, 98, 78-90 (2018).
- [20] Avvari P.V., Yang Y., and Soh C.K., "Long-term fatigue behavior of a cantilever piezoelectric energy harvester," Journal of Intelligent Material Systems and Structures, 28, 1188-1210 (2017).
- [21] Soma A., De Pasquale G. 2013 Design of high-efficiency vibration energy harvesters and experimental functional tests for improving bandwidth and tunability. In *Smart Sensors, Actuators, and MEMS VI. International Society for Optics and Photonics*; Grenoble.
- [22] Ferrari M., Ferrari V., Guizzetti M., Andò B., Baglio S., and Trigona C., "Improved energy harvesting from wideband vibrations by nonlinear piezoelectric converters," Sensors and Actuators A: Physical, 162, 425-431 (2010).
- [23] Erturk A., Hoffmann J., and Inman D.J., "A piezomagnetoelastic structure for broadband vibration energy harvesting," Applied Physics Letters, **94**, 254102 (2009).
- [24] Harne R.L., Wang K.W., "A review of the recent research on vibration energy harvesting via bistable systems," Smart Materials and Structures, **22**, 023001 (2013).
- [25] Haupt R.L., Haupt S.E., [Practical genetic algorithms], Wiley, New York, (1998).